VIP High-Spin Keggin Systems

DOI: 10.1002/anie.201100515

Redox-Controlled Magnetic {Mn_{13}} Keggin Systems**

*Graham N. Newton, Satoshi Yamashita, Koen Hasumi, Junzo Matsuno, Norifumi Yoshida, Masayuki Nihei, Takuya Shiga, Motohiro Nakano, Hiroyuki Nojiri, Wolfgang Wernsdorfer, and Hiroki Oshio**

Polyoxometalates (POMs) have been widely reported in recent years. These molecular metal oxides, or polyanions, are most commonly constructed of tungsten, molybdenum, or vanadium ions in their highest oxidation state, bridged by oxide ligands to form clusters which can range in size from low-nuclearity building blocks to large-scale protein-like superstructures.[1] An archetypical POM structural motif is the $\{XM_{12}O_{40}\}^{n-}$ species (X = P, Si…) known as the Keggin anion and Keggin structures have been successfully shown to act as catalysts[2] among other potential applications.[3] POMs are inorganic materials that can be functionalized through their combination with organic ligands and/or the introduction of paramagnetic heterometal ions which leads to magnetic heterometallic POMs.[4–6] In addition, there are a few studies of related species consisting exclusively of late first-row transition-metal ions such as some mixed-valence manganese Keggin-related clusters described by Lampropoulos et al,[7] the uncapped {Fe_{13}} cluster reported by Bino et al.,[8] and the reverse-Keggin structures presented by Baskar et al.[9] To the best of our knowledge, there are no other examples of POM-type complexes consisting exclusively of open-shell transition metals, and so far their physical properties have been barely investigated. In contrast, transition-metal oxide materials are widely used and their properties such as magnetic ordering, semi- and superconductivity, giant magnetoresistance, and ferroelectricity are much studied. Their electronic properties can be understood by their band structures and changed to show the desired characteristics.[10,11] Replication or improvement of metal oxide properties in discrete molecules can be extremely difficult. However, molecular metal clusters can possess well-separated energy levels and their characteristic electronic structures can be altered to show, for example, valence tautomerism, multi-bistability with spin crossover, and single-molecule-magnetic (SMM) behavior by tuning the frontier orbitals and the electronic interactions between the metal centers.[12–15] The band filling in solids is readily controlled in their syntheses by altering the ratio of the constituent elements which drastically changes the physical properties. The question arises whether the chemist can synthesize metal oxide clusters displaying controllable redox states which can perturb the physical properties.

Herein, a polyoxometalate-type cluster was synthesized by using exclusively first-row transition-metal ions in combination with organic capping ligands. In the resultant system the spin state and magnetic properties were tuned without substantial change to the molecular structure, and its SMM behavior was perturbed through manipulation of the cluster oxidation state. Herein, the synthesis, magnetic properties, and redox behavior of three mixed-valence {Mn_{13}} Keggin-type clusters are reported.

The one-pot reaction of $Mn(NO_3)_2{\cdot}6H_2O$ with 2,6-bis[*N*-(2-hydroxyethyl)iminomethyl]-4-methylphenol (H_3bemp)[16] in methanol yielded a tridecanuclear cluster $[Mn^{III}{}_{12}Mn^{IV}O_6(OH)_2(OMe)_4(bemp)_6]$-$(NO_3)_4{\cdot}10MeOH{\cdot}6H_2O$ (**1(NO$_3$)$_4$**) (Figure 1 and Figure S1 in the Supporting Information). Subsequent high-yielding crystallization led to the formation of dark brown square blocks of **1(NO$_3$)$_4$**, the counterions of which were exchanged to yield **1(PF$_6$)$_4$** from a solution of **1(NO$_3$)$_4$** and NH_4PF_6 in methanol. The core structure and physical behavior of **1(PF$_6$)$_4$** were identical to **1(NO$_3$)$_4$**. Dark brown platelets of **1(PF$_6$)$_4$** were then dissolved in methanol with one or two equivalents of $[Fe^{III}(bpy)_3](PF_6)_3$ (bpy = 2,2′-bipyridine) to yield dark brown rhombic crystals of oxidized **1(PF$_6$)$_5$** and **1(PF$_6$)$_6$**, respectively.[17]

Cyclic voltammetry (CV) measurements conducted on **1(NO$_3$)$_4$** (1 mM) in *N*,*N*-dimethylformamide (DMF) showed four quasireversible waves at 0.02, 0.18, 0.50, and 0.73 V versus the saturated calomel electrode (SCE), corresponding to four one-electron redox processes of $\mathbf{1}^{2+}/\mathbf{1}^{3+}$, $\mathbf{1}^{3+}/\mathbf{1}^{4+}$, $\mathbf{1}^{4+}/\mathbf{1}^{5+}$, and $\mathbf{1}^{5+}/\mathbf{1}^{6+}$, respectively (Figure 2). Approximating the complex as a trinuclear redox-active system, we calculated comproportionation constants of 560, 2.6×10^5, and 5.5×10^3 for the reduced $\mathbf{1}^{3+}$ ($Mn^{II}Mn^{III}{}_{11}Mn^{IV}$), the native species $\mathbf{1}^{4+}$ ($Mn^{III}{}_{12}Mn^{IV}$), and the oxidation product $\mathbf{1}^{5+}$ ($Mn^{III}{}_{11}Mn^{IV}{}_2$),

[*] Dr. G. N. Newton, S. Yamashita, K. Hasumi, J. Matsuno, N. Yoshida, Dr. M. Nihei, Dr. T. Shiga, Prof. Dr. H. Oshio
Graduate School of Pure and Applied Sciences
University of Tsukuba
Tennodai 1-1-1, Tsukuba 305-8571 (Japan)
Fax: (+81) 29-853-4238
E-mail: oshio@chem.tsukuba.ac.jp
Prof. Dr. M. Nakano
Department of Applied Chemistry
Graduate School of Engineering, Osaka University
2-1 Yamada-oka, Suita, Osaka 565-0871 (Japan)
Prof. Dr. H. Nojiri
Institute of Material Research, Tohoku University
Katahira 2-1-1, Aoba-ku, Sendai 980-8577 (Japan)
Dr. W. Wernsdorfer
Institut Néel, CNRS & Université J. Fourier
BP166, 25 Rue des Martyrs, 38042 Grenoble Cedex 9 (France)

[**] This work was supported by a grant-in-aid for scientific research and for the priority area "Coordination Programming" (area 2107) from the MEXT (Japan) and the JSPS.

Supporting information for this article is available on the WWW under http://dx.doi.org/10.1002/anie.201100515.

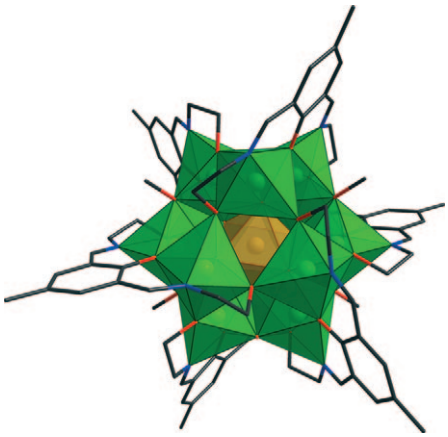

Figure 1. The tridecanuclear complex $\mathbf{1(NO_3)_4}$. The Mn^{III} polyhedra are given in green, the Mn^{IV} polyhedron in gold, the O centers in red, C in dark gray, and N in blue. The hydrogen atoms and counteranions have been omitted for clarity.

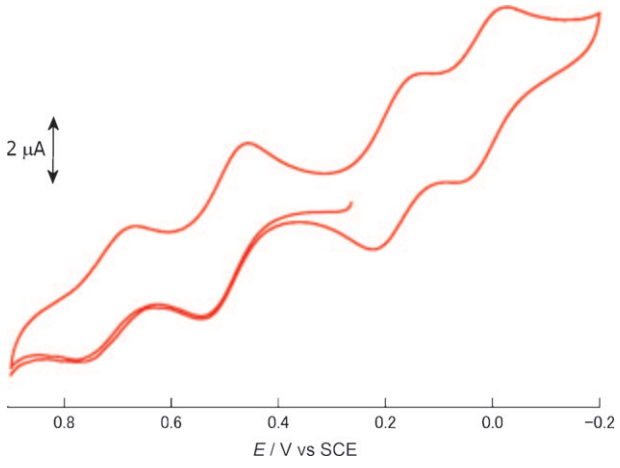

Figure 2. Cyclic voltammogram of $\mathbf{1(NO_3)_4}$ in DMF, using TBA·PF_6 as the electrolyte under N_2 at a scan rate of 0.01 Vs^{-1}.

respectively.[18] The four reversible waves suggest that **1** can exist in five stable oxidation states; herein, we describe the isolation and characterization of complexes in three of these oxidation states.

The core of $\mathbf{1(NO_3)_4}$ consists of three layers: a heptanuclear disc and two identical trinuclear caps (see Figure S2 in the Supporting Information). The heptanuclear unit comprises a Mn^{III}_6 hexagon with a central templating Mn^{IV} ion, while the two Mn^{III}_3 triangular units lie flat above and below the disc. The central Mn^{IV} is coordinated to six μ_4-oxide ions, (average Mn–O distances of 1.896(5) Å) which each link the Mn^{IV} ion to two Mn^{III} ions from the hexagonal ring and one from a vertex of the triangular capping units. The hexagonal ring of seven-coordinate Mn^{III} centers is additionally bridged by two hydroxide and four methoxide anions, and the coordination environments of the metals are completed by six $bemp^{3-}$ ligands, each of which coordinates four Mn^{III} ions. The seven-coordinate Mn^{III} ions have two elongated Mn–O bonds (average bond length of 2.458(5) Å) and one relatively long $Mn–N_{imine}$ bond (average distance of 2.270(5) Å). The Mn–O bonds which form the ring of the hexagonal unit through hydroxo and methoxo ligands display Jahn–Teller compression with average distances of 1.912(4) Å, while the remaining two coordination sites are occupied by one oxo and one phenoxo group with an average bond length of 1.991(4) Å. In the trinuclear capping units all the Mn^{III} centers show Jahn–Teller elongation along the plane of the triangle in the interactions with one alkoxo and one phenoxo donor (average Mn–O distance of 2.181(4) Å). The octahedral coordination environment is completed by three Mn^{III}–O bonds and one Mn^{III}–N bond (average distances of 1.918(4) and 1.990(5) Å, respectively). Bond valence sum (BVS) calculations and the charge balance strongly suggest that the central ion is in the IV+ oxidation state while all other ions are in the III+ oxidation state.[19]

The central $Mn^{IV}O_6$ unit forms oxo bridges to all 12 Mn^{III} centers, thus templating the cluster, while the $bemp^{3-}$ ligands and the hydroxo/methoxo bridges decorate the outside of the complex. The presence of four transition-metal "triads" coordinated around a central templating octahedrally coordinated metal center suggests that $\mathbf{1(NO_3)_4}$ can be considered a distorted α-Keggin-type species (see Figure S3 in the Supporting Information). Classical α-Keggin anions have idealized tetrahedral (T_d) symmetry and are composed of $\{M_3O_{13}\}$ triads.[20] Furthermore, the surfaces of these molecular metal oxides are composed of nonbasic terminal M=O bonds, whereas the majority of the donor atoms in $\mathbf{1(NO_3)_4}$ are alkoxo and phenoxo ligands. The oxidized clusters $\mathbf{1(PF_6)_5}$ and $\mathbf{1(PF_6)_6}$ are isotopological to $\mathbf{1(NO_3)_4}$; however, their bonds around one of the manganese centers (Mn(2) and Mn(9) in $\mathbf{1(PF_6)_5}$ and Mn(2) for $\mathbf{1(PF_6)_6}$, and their symmetry generated equivalents (Mn(2)′ and Mn(9)′) in the trinuclear capping units are shorter than in $\mathbf{1(NO_3)_4}$, with an average Mn(2/9)–O/N distance of 1.987(4) Å (BVS = 3.47) for $\mathbf{1(PF_6)_5}$ and a Mn(2)–O/N distance of 1.926(6) Å (BVS = 3.98) for $\mathbf{1(PF_6)_6}$ (see Figure S4 in the Supporting Information). The observed bond lengths, BVS calculations, and the charge balance suggest valences of 3.5+ (disordered over two positions) for $\mathbf{1(PF_6)_5}$ and 4+ for $\mathbf{1(PF_6)_6}$.[19]

The magnetic susceptibilities of powder samples of $\mathbf{1(NO_3)_4}$, $\mathbf{1(PF_6)_5}$, and $\mathbf{1(PF_6)_6}$ were measured in the temperature range of 1.8–300 K under an external magnetic field of 0.05 Tesla (see Figure S5 in the Supporting Information). The $\chi_m T$ value at 300 K is 39.26 $emu\,mol^{-1}\,K$ for $\mathbf{1(NO_3)_4}$, 40.28 $emu\,mol^{-1}\,K$ for $\mathbf{1(PF_6)_5}$, and 40.36 $emu\,mol^{-1}\,K$ for $\mathbf{1(PF_6)_6}$; all values are larger than the $\chi_m T$ values expected from the magnetically independent manganese ions in $\{Mn^{III}_{12}Mn^{IV}\}$, $\{Mn^{III}_{11}Mn^{IV}_2\}$, and $\{Mn^{III}_{10}Mn^{IV}_3\}$ clusters (37.88, 36.75, and 35.63 $emu\,mol^{-1}\,K$, respectively, with a Landé factor (g) of 2.0). Similar temperature profiles of the $\chi_m T$ values were observed for the three complexes and the $\chi_m T$ values increased gradually as the temperature was lowered, reaching maximum values of 42.08, 42.42, and 42.42 $emu\,mol^{-1}\,K$ at 120, 132, and 156 K, respectively. Below the maximum, the $\chi_m T$ values decreased, reaching minima of 9.51, 13.16, and 16.66 $emu\,mol^{-1}\,K$ at 1.8 K. The slight increases in the high-temperature ranges indicate ferromagnetic interactions between manganese ions. However, the decrease in the $\chi_m T$ value below 100 K is due to

antiferromagnetic interactions and magnetic anisotropy. Although **1(PF$_6$)$_6$** has the least number of unpaired electrons of the three compounds, its $\chi_m T$ value is larger than that of the others at 1.8 K. When the $\chi_m T$ values in the low-temperature region are compared, the $\chi_m T$ values are larger for the molecular cations with the higher oxidation states, suggesting that the spin quantum numbers of the ground states increase after the oxidation, which is supported by the $\chi_m' T$ versus T plots (see Figure S5 and its inset in the Supporting Information). All compounds show linearity of the $\chi_m' T$ values in the region from 3 to 4 K, and extrapolations to 0 K give $\chi_m' T$ values of 11.03, 13.05, and 14.65 emu mol^{-1} K for **1-(NO$_3$)$_4$**, **1(PF$_6$)$_5$**, and **1(PF$_6$)$_6$**, which are close to the values expected for $S = 9/2$, 10/2, and 11/2, respectively, supposing a g value of 2. Interpretations of the magnetic properties are not straightforward. The magnetic interactions between manganese ions of the central {Mn$_7$} wheel can be considered relatively strong as a consequence of the oxo-bridged magnetic paths, while those in the triangular {Mn$_3$} units are relatively weak as a result of the alkoxo and hydroxo bridges between the metal centers. Since both interactions have the potential to induce spin frustration, the observable magnetic moments cannot be accurately predicted by classical antiferromagnetic interactions. Crystallographic studies revealed that the manganese ions of the triangular {Mn$_3$} units are oxidized in **1**$^{5+}$ and **1**$^{6+}$ while the total spin number of the clusters increases. The spins belonging to the {Mn$_3$} triangles align against the direction of the total resultant spin because of the strong antiferromagnetic interactions with the central {Mn$_7$} wheel unit. Therefore, the spin ground states are expected to be higher for the more oxidized species which have fewer spins on the triangle units.

The alternating-current (ac) magnetic susceptibilities of all complexes show distinct frequency-dependent responses of both in- and out-of-phase signals, which is indicative of SMM behavior (see Figure S6 in the Supporting Information). The ac response becomes more remarkable with increasing oxidation state as confirmed by the Cole–Cole and Arrhenius plots (see Figure S7 in the Supporting Information);[21] however, the peak tops could not be observed above 1.8 K. By using a micro-SQUID (SQUID = semiconducting quantum interference device)[22] for hysteresis measurements on aligned single crystals of **1(PF$_6$)$_4$**, **1(PF$_6$)$_5$**, and **1(PF$_6$)$_6$**, we observed both the scan rate, from 0.001 to 0.560 T s^{-1}, and the temperature dependence, from 0.04 to 1 K, on the hysteretic responses (see Figure 3 and Figure S8 in the Supporting Information). All three samples showed responses in which the hysteresis widened with increasing sweep rate and lowered temperature, and clear steps appeared in the curves of the oxidized species. The results suggest that the blocking temperatures of the compounds increased with higher oxidation states, displaying broader and more clearly stepped hysteresis loops, which is in agreement with the estimated blocking temperatures.[21]

The compounds are SMMs and must have easy-axis-type magnetic anisotropy ($D < 0$). The Mn^{III} ions on the triangles show Jahn–Teller elongation, suggesting negative D values for the single ions. However, their Jahn–Teller axes are aligned along the planes of the triangles with torsion angles of

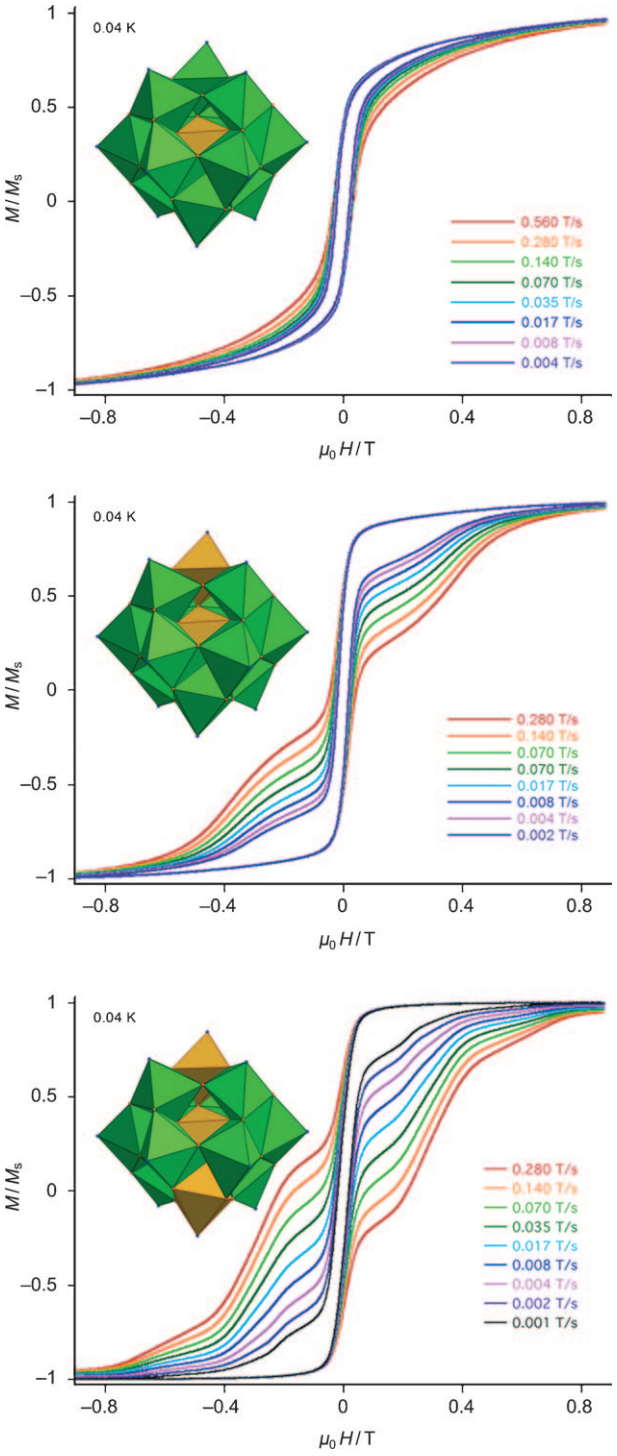

Figure 3. Micro-SQUID hysteresis measurements displaying the scan-rate dependence for **1(PF$_6$)$_4$** (top), **1(PF$_6$)$_5$** (middle), and **1(PF$_6$)$_6$** (bottom). The insets show cluster cores with green and brown polyhedra around the Mn^{III} and Mn^{IV} ions, respectively. The Mn^{IV} ion in the triangle of **1(PF$_6$)$_5$** is positionally disordered between both triangles with a population of 0.5.

16.27–17.49°, which classically results in $D > 0$ for both triangular units.[23] Therefore, the overall D value of the central hexagon must be negative. The angular overlap model (AOM) calculations for the seven coordinated Mn^{III} ions on

the central heptanuclear unit suggest that each Mn^{III} ion has a hard axis ($D > 0$; see Figure S9 in the Supporting Information). The hard axes, however, are aligned along the outer ring of the hexagon through the contracted Mn–O bonds, resulting in an overall easy-axis normal to the plane of the heptanuclear unit (see Figure S10 in the Supporting Information). It can be presumed that the overall magnetic anisotropy of the clusters is of easy-axis type, dominated by that of the heptanuclear units. When the cluster oxidation state is raised and isotropic Mn^{IV} centers replace Mn^{III} ions in the triangular units, the $D > 0$ contribution of the triangles lessens, increasing the overall negative D value for the cluster. The higher blocking temperature for the oxidized molecules can be understood by the higher spin ground states and the larger anisotropy accessed through the oxidation. The magnetic behavior of redox-active SMMs can be gradually altered through changes to the oxidation state of a cluster. Electrochemically isolated $[Mn^{III}{}_3Mn^{IV}]$ moieties showed the onset of SMM properties with oxidation (and structural alteration),[24,25] and our results are analogous to studies on $\{Mn_{12}\}$ SMMs which showed a decrease in the effective energy barrier through stepwise reduction.[26] Our findings act as a good comparison to previous studies because the structural integrity is retained during the stepwise oxidation leading to an enhancement of the magnetic response.

In conclusion, a family of mixed valence $\{Mn_{13}\}$ Keggin-type clusters was synthesized, displaying switchable redox behavior while the structural integrity is retained. Three different oxidation states of the cluster were isolated and characterized by crystallography and magnetic susceptibility measurements, confirming the one-electron oxidation events which distinguish the three species. All clusters display similar SMM behavior observed for the first time in homometallic Keggin-type clusters. This behavior is amplified as the clusters are oxidized. We have presented a first study on the electronic structure of manganese α-Keggin systems which have shown stable redox activity and interesting magnetic properties. This study provides a starting point for research of first-row transition-metal POM-type clusters, and future work with, for example, iron and cobalt ions, or mixtures of metals, may allow access to species with new functionalities and physical properties.

Experimental Section

Synthesis: All reagents were obtained from commercial suppliers and were used without further purification. The ligand 2,6-bis-[*N*-(2-hydroxyphenyl)iminomethyl]-4-methylphenol (H_3bemp) was prepared by a literature method.[16]

$1(NO_3)_4$·10 MeOH·6 H_2O: $Mn(NO_3)_2$·6 H_2O (2870 mg, 10 mmol) in methanol (50 mL) was added to a mixture of 2,6-diformyl-4-methylphenol (820 mg, 5 mmol) and 2-aminoethanol (610 mg, 10 mmol) in methanol (100 mL). The reaction mixture was heated to reflux at 60 °C for 20 minutes and then allowed to cool to room temperature. Triethylamine (1520 mg, 15 mmol) in methanol (50 mL) was added to the solution. The resulting brown solution was again heated to reflux for 20 minutes and then kept at room temperature for a few days to yield dark brown square plates of **$1(NO_3)_4$**·10 MeOH·6 H_2O which are suitable for single-crystal X-ray analysis. The brown crystals were collected by filtration and dried in air to give **$1(NO_3)_4$**·6 H_2O (yield 60%); elemental analysis calcd (%) for $C_{82}H_{116}N_{16}O_{48}Mn_{13}$: C 35.07, H 4.16, N 7.98; found: C 34.53, H 3.99, N 7.93.

$1(PF_6)_5$·Et_2O·1.5 MeOH·4 MeCN·2 H_2O: A stirred dark brown solution of **$1(PF_6)_4$** (78.5 mg, 0.025 mmol) in CH_3CN/MeOH (10 mL, 5:1 v/v) was treated with $[Fe^{III}(bpy)_3](PF_6)_3$ (25 mg, 0.025 mmol) and the mixture was stirred for 30 minutes, then filtered, and layered with Et_2O (15 mL). After six days, dark red parallelopipeds of **$1(PF_6)_5$**·Et_2O·1.5 MeOH·4 MeCN·2 H_2O (45%) were collected by filtration; elemental analysis calcd (%) for dried **$1(PF_6)_5$**·2 H_2O, $C_{78}H_{100}N_{12}O_{32}P_5F_{30}Mn_{13}$: C 29.67, H 3.19, N 5.32; found: C 29.49, H 3.27, N 5.40.

$1(PF_6)_6$·2 MeOH·10 MeCN·2 H_2O: The procedure is similar to the preparation of **$1(PF_6)_5$**. A stirred dark brown solution of **$1(PF_6)_4$** (78.5 mg, 0.025 mmol) in CH_3CN/MeOH (10 mL, 5:1 v/v) was treated with $[Fe^{III}(bpy)_3](PF_6)_3$ (50 mg, 0.050 mmol) and the mixture was stirred for 30 minutes. The solution was filtered and layered with Et_2O (15 mL). After six days, dark red parallelopipeds of **$1(PF_6)_6$**·2 MeOH·10 MeCN·2 H_2O (40%) were collected by filtration; elemental analysis calcd (%) for dried **$1(PF_6)_6$**·2 H_2O, $C_{78}H_{100}N_{12}O_{32}P_6F_{36}Mn_{13}$: C 28.37, H 3.05, N 5.09; found: C 28.55, H 3.24, N 5.16.

Received: January 21, 2011
Published online: April 15, 2011

Keywords: Keggin systems · manganese · polyoxometalates · redox chemistry · single-molecule studies

[1] D.-L. Long, R. Tsunashima, L. Cronin, *Angew. Chem.* **2010**, *122*, 1780–1803; *Angew. Chem. Int. Ed.* **2010**, *49*, 1736–1758.
[2] K. Kamata, K. Yonehara, Y. Nakagawa, K. Uehara, N. Mizuno, *Nat. Chem.* **2010**, *2*, 478–483.
[3] E. Coronado, C. J. Gomez-Garcia, *Chem. Rev.* **1998**, *98*, 273–296.
[4] K.-Y. Choi, N. S. Dalal, A. P. Reyes, P. L. Kuhns, Y. H. Matsuda, H. Nojiri, S. S. Mal, U. Kortz, *Phys. Rev. B* **2008**, *77*, 024406.
[5] C. Ritchie, A. Ferguson, H. Nojiri, H. N. Miras, Y.-F. Song, D.-L. Long, E. Burkholder, M. Murrie, P. Kögerler, E. K. Brechin, L. Cronin, *Angew. Chem.* **2008**, *120*, 5691–5694; *Angew. Chem. Int. Ed.* **2008**, *47*, 5609–5612.
[6] M. A. AlDamen, J. M. Clemente-Juan, E. Coronado, C. Martí-Gastaldo, A. Gaita-Ariño, *J. Am. Chem. Soc.* **2008**, *130*, 8874–8875.
[7] C. Lampropoulos, M. Murugesu, K. A. Abboud, G. Christou, *Polyhedron* **2007**, *26*, 2129–2134.
[8] A. Bino, M. Ardon, D. Lee, B. Spingler, S. J. Lippard, *J. Am. Chem. Soc.* **2002**, *124*, 4578–4579.
[9] V. Baskar, M. Shanmugam, M. Helliwell, S. J. Teat, R. E. P. Winpenny, *J. Am. Chem. Soc.* **2007**, *129*, 3042–3043.
[10] P. J. Hagrman, D. Hagrman, J. Zubieta, *Angew. Chem.* **1999**, *111*, 2798–2848; *Angew. Chem. Int. Ed.* **1999**, *38*, 2638–2684.
[11] M. Imada, A. Fujimori, Y. Tokura, *Rev. Mod. Phys.* **1998**, *70*, 4, 1039–1263.
[12] R. W. Saalfrank, R. Prakash, H. Maid, F. Hampel, F. W. Heinemann, A. X. Trautwein, L. H. Böttger, *Chem. Eur. J.* **2006**, *12*, 2428–2433.
[13] M. Nihei, H. Tahira, N. Takahashi, Y. Otake, Y. Yamamura, K. Saito, H. Oshio, *J. Am. Chem. Soc.* **2010**, *132*, 3553–3560.
[14] R. Sessoli, D. Gatteschi, A. Caneschi, M. A. Novak, *Nature* **1993**, *365*,141–143.
[15] V. Balzani, A. Juris, M. Venturi, *Chem. Rev.* **1996**, *96*, 759–833.
[16] W.-X. Zhang, C.-Q. Ma, X.-N. Wang, Z.-G. Yu, Q. - *J.* Lin, D.-H. Jiang, *Chin. J. Chem.* **1995**, 13, 497–503.
[17] Crystal structure data for **$1(NO_3)_4$**·10 (CH_3OH)·6 (H_2O): $C_{92}H_{156}N_{16}O_{58}Mn_{13}$, 3128.49 g mol^{-1}, triclinic $P\bar{1}$, $a = 13.276(7)$, $b = 16.367(9)$, $c = 17.462(9)$ Å, $\alpha = 113.922(11)$, $\beta = 110.714(11)$,

$\gamma = 95.624(11)$ deg, $V = 3112(3)$ Å^3, $Z = 1$, final $R1 = 0.0526$, $wR2 = 0.1547$ ($I > 2\sigma(I)$). Disordered solvent molecules in the crystal voids were removed from calculations by the SQUEEZE program in the PLATON suite; **1(PF$_6$)$_5$**·(Et_2O)·1.5(MeOH)·4(MeCN)·2(H_2O): $C_{91\cdot5}H_{128}F_{30}Mn_{13}N_{16}O_{34\cdot50}P_5$, 3443.10 g mol^{-1}, triclinic $P\bar{1}$, $a = 15.202(2)$, $b = 17.345(3)$, $c = 29.375(5)$ Å, $\alpha = 83.862(3)$, $\beta = 86.522(3)$, $\gamma = 67.482(3)$ deg, $V = 7112.6(19)$ Å^3, $Z = 2$, final $R1 = 0.0451$, $wR2 = 0.1274$ ($I > 2\sigma(I)$). Disordered solvent molecules in the crystal voids removed from calculations by the SQUEEZE program in the PLATON suite; **1(PF$_6$)$_6$**·2(CH_3OH)·10(CH_3CN)·2(H_2O): $C_{100}H_{138}F_{36}Mn_{13}N_{22}O_{34}P_6$, 3776.36 g mol^{-1}, monoclinic $C2/c$, $a = 30.026(7)$, $b = 18.074(7)$, $c = 28.920(9)$ Å, $\beta = 113.143(11)$ deg, $V = 14432(8)$ Å^3, $Z = 4$, final $R1 = 0.0639$, $wR2 = 0.1818$ ($I > 2\sigma(I)$). The crystallographic formulae have been amended in **1(NO$_3$)$_4$** and **1(PF$_6$)$_5$** to include the number of solvent molecules suggested by SQUEEZE (see cif files). CCDC 808811 **1(NO$_3$)$_4$**, 808812 **1(PF$_6$)$_5$** and 808813 **1(PF$_6$)$_6$** contain the supplementary crystallographic data for this article. These data can be obtained free of charge from The Cambridge Crystallographic Data Centre via www.ccdc.cam.ac.uk/data_request/cif.

[18] D. M. D'Alessandro, F. R. Keene, *Chem. Rev.* **2006**, *106*, 2270 – 2298.

[19] BVS for **1(NO$_3$)$_4$**: Mn1 = 4.08; Mn2 = 3.25; Mn3 = 3.27; Mn4 = 3.16; Mn5 = 3.01; Mn6 = 3.06; Mn7 = 2.96. **1(PF$_6$)$_5$**: Mn1 = 4.23; Mn2 = 3.49; Mn3 = 3.26; Mn4 = 3.19; Mn5 = 3.06; Mn6 = 3.07; Mn7 = 3.04; Mn8 = 4.30; Mn9 = 3.43; Mn10 = 3.35; Mn11 = 3.22; Mn12 = 3.09; Mn13 = 3.08; Mn14 = 3.03. **1(PF$_6$)$_6$**: Mn1 = 4.30; Mn2 = 3.99; Mn3 = 3.26; Mn4 = 3.22; Mn5 = 3.14; Mn6 = 3.07; Mn7 = 3.12.

[20] P. Mialane, A. Dolbecq, L. Lisnard, A. Mallard, J. Marrot, F. Sécheresse, *Angew. Chem.* **2002**, *114*, 2504 – 2507; *Angew. Chem. Int. Ed.* **2002**, *41*, 2398 – 2401.

[21] The Cole–Cole plots of these data were analyzed by the Debye model, and the effective energy barriers (ΔE) and pre-exponential factors (τ_0) given by their Arrhenius plots (see Figure S7 in the Supporting Information), resulting in $\Delta E = 3.6(3)$ K, $\tau_0 = 10(2) \times 10^{-6}$ s for **1(NO$_3$)$_4$**, $\Delta E = 7.9(9)$ K, $\tau_0 = 6(2) \times 10^{-7}$ s for **1(PF$_6$)$_5$**, and $\Delta E = 14.1(9)$ K, $\tau_0 = 3(2) \times 10^{-8}$ s for **1(PF$_6$)$_6$**, respectively. The blocking temperatures (with $\tau = 100$ s) were approximately 0.2 K for **1(NO$_3$)$_4$**, 0.4 K for **1(PF$_6$)$_5$**, and 0.6 K for **1(PF$_6$)$_6$**.

[22] W. Wernsdorfer, K. Hasselbach, A. Benoit, B. Barbara, D. Mailly, J. Tuaillon, J. P. Perez, V. Dupuis, J. P. Dupin, G. Guiraud, A. Perex, *J. Appl. Phys.* **1995**, 78, 7192 – 7195.

[23] H. Oshio, M. Nakano, *Chem. Eur. J.* **2005**, *11*, 5178 – 5185.

[24] S. Wang, M. S. Wemple, J. Yoo, K. Folting, J. C. Huffman, K. S. Hagen, D. N. Hendrickson, G. Christou, *Inorg. Chem.* **2000**, *39*, 1501 – 1513.

[25] N. Aliaga-Alcalde, R. S. Edwards, S. O. Hill, W. Wernsdorfer, K. Folting, G. Christou, *J. Am. Chem. Soc.* **2004**, *126*, 12503 – 12516.

[26] M. Soler, W. Wernsdorfer, K. A. Abboud, J. C. Huffman, E. R. Davidson, D. N. Hendrickson, G. Christou, *J. Am. Chem. Soc.* **2003**, *125*, 3576 – 3588.

